THE JOURNAL OF PHYSICAL CHEMISTRY C
A JOURNAL OF THE AMERICAN CHEMICAL SOCIETY

pubs.acs.org/JPCC

Article

# "Liquid-like" Water in Clathrates Induced by Host–Guest Hydrogen Bonding

Ngoc N. Nguyen,* Rüdiger Berger,* Manfred Wagner, Jürgen Thiel, Hans-Jürgen Butt, and Robert Graf*

Cite This: *J. Phys. Chem. C* 2021, 125, 15751–15757

Read Online

ACCESS | Metrics & More | Article Recommendations | Supporting Information

**ABSTRACT:** Clathrate structures are sustained by a host lattice formed by hydrogen-bonding water molecules, which encapsulates guest molecules. Up to now, all water molecules in the host lattice are considered ice-like crystallized. Here, we discovered the occurrence of "liquid-like" water molecules and the resulting defects in (polar) tetrahydrofuran clathrates by liquid-state $^{1}$H NMR experiments. The liquid-like water molecules start occurring at 271 K, well below the apparent dissociation point (277 K) of the clathrate matrix, via extracting water molecules from the host lattice by host–guest H-bonding. We found an intriguing two-stage dissociation of the clathrate: Partial dissociation at 271 K converting one-third of water molecules into liquid-like followed by complete dissociation at 277 K. The clathrate structure is molecularly heterogeneous in the region between 271 K and 277 K. No liquid-like water exists in (nonpolar) cyclopentane clathrates. This work uncovers the essentiality of host–guest interaction for clathrate structures and the ability to tune their stability using polar molecules.

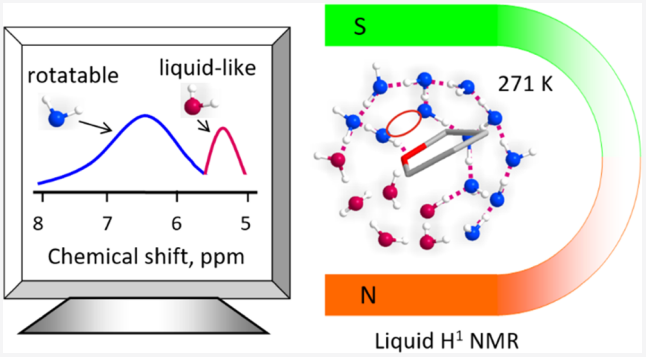




## 1. INTRODUCTION

Clathrates are considered as the next-generation material for fuel gas storage.[1−4] They are host–guest inclusion structures in which water molecules coordinate via hydrogen bonding (H-bonding) to form a cage-like framework that serves as a host structure.[5] "Guest" molecules with suitable sizes are incorporated into the regular cavities of the host structure.[5,6] In this way, the largest part of methane on Earth is encapsulated in natural clathrates, commonly named as combustible ice,[7−9] which constitute a vast untapped source of low-carbon energy that is far cleaner than oil and coal.[7,8,10−13] Meanwhile, synthetic clathrates offer a rare opportunity for technical fuel gas storage.[14] Fuel gas such as methane and hydrogen can be encapsulated in the cavities of clathrate structures at mole fractions in the order of 0.1.

Clathrates containing polar guests offer an effective gas-storing material since they form at low pressures. In particular, polar guests such as tetrahydrofuran (THF) and dioxolane form clathrates already at atmospheric pressures.[14−17] Recently, a better hydrogen storage was attained by the inclusion of perchloric acid as an additive to THF clathrate.[18] In principle, polar molecules might induce additional defects in the host lattice that facilitate the uptake and diffusion of fuel gas molecules in the clathrate. Therefore, defects in the host lattice may play a key role in determining gas storage. Classical understanding of clathrates is based on nonpolar guest molecules, for which structural defects are not considered since nonpolar guest molecules do not interfere the host lattice strongly. For polar guest molecules such as THF, temporary host–guest H-bonds can be sufficient to interfere the intrinsic water–water H-bonds[19−22] and create H-bonding defects in the host lattice, known as Bjerrum defects.[23−26]

However, to what extent the polar guest molecules affect the structure and stability of the clathrates is still unknown. Previous probes of clathrate structures were based primarily on solid-state techniques, which are sensitive to immobile (crystallized) water molecules that have permanent H-bonds. Typically, defects in clathrates were investigated at temperatures below 200 K since at higher temperatures, the reorientation of water molecules becomes too fast for solid-state techniques such as $^{2}$H solid-state nuclear magnetic resonance (NMR).[23,25−27] At such low temperatures, water molecules in the host structure are ice-like crystallized and the influence of host–guest interaction is not critical to the stability of the clathrates. In contrast, the temperature region

**Received:** June 23, 2021
**Revised:** June 27, 2021
**Published:** July 12, 2021

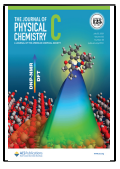





https://doi.org/10.1021/acs.jpcc.1c05531
*J. Phys. Chem. C* 2021, 125, 15751–15757

around 273 K involves the formation and dissociation of clathrates and is thus of central importance. However, the structure of clathrates in this temperature region remains almost untapped. In particular, it is not known to what extent host−guest H-bonding and Bjerrum defect influence the stability and phase transitions of clathrate structures.

Here, we employed liquid-state $^1$H NMR (hereafter, $^1$H NMR) to probe the structure of clathrates depending on host−guest interactions at temperatures crossing the clathrate dissociation region. We used cyclopentane and THF clathrates. Cyclopentane and THF have similar molecular sizes, shapes, and molecular weights but different polarities. Cyclopentane is nonpolar, whereas THF is polar. These clathrates are, therefore, ideal for comparing the influence of host−guest interactions on clathrate structures. We used the liquid $^1$H NMR method because it is sensitive to mobile water molecules, i.e., water molecules with H-bonds fluctuating on the microsecond to millisecond time scale. Immobile water molecules having permanent H-bonds with their neighbors are observed only as a broad spectral background.[28] We discovered the occurrence of "liquid-like" water molecules in the THF clathrate starting at 271 K, well below the apparent equilibrium dissociation point (277 K) of the clathrate matrix, and quantified their fraction as a function of the temperature. The THF clathrate dissociates in two stages. We propose a molecular structure of THF clathrates as a function of the temperature.

## 2. METHODS

**Materials.** Materials used were deuterated tetrahydrofuran (THF-$d_8$, $C_4D_8O$ 99.5 atom %D, Carl Roth GmbH), deuterated cyclopentane-$d_{10}$ ($C_5D_{10}$ 99 atom %D, Sigma-Aldrich), protonated tetrahydrofuran (THF, $C_4H_8O$ 99.8%, Sigma-Aldrich), protonated cyclopentane ($C_5H_{10}$ 99.8%, Fisher Scientific), deuterated methylene chloride ($CD_2Cl_2$, 99.5 atom %D, Sigma-Aldrich), methylene chloride ($CH_2Cl_2$ 99.5%, Sigma-Aldrich), deuterated acetone-$d_6$ ($C_2D_6O$ 99 atom %D, Sigma-Aldrich), and protonated acetone ($C_2H_6O$ 99%, Sigma-Aldrich).

**Experimental Procedures.** We used clathrates of deuterated THF (THF-$d_8$, $C_4D_8O$) and cyclopentane-$d_{10}$ ($C_5D_{10}$) to avoid the interference of the H atoms on the guest molecules. Clathrates of protonated THF ($C_4H_8O$) and protonated cyclopentane ($C_5H_{10}$) were only examined for comparison in some cases.

*Preparation of Clathrate Samples.* THF-$d_8$ clathrates were prepared via slow crystallization of a stoichiometric solution (water/THF-$d_8$ = 17/1 mole ratio) at 0 °C and ambient pressure. Ice baths were used to maintain the temperature at 0 °C. NMR tubes made of Teflon were filled with the THF-$d_8$ solution (Figure 1a). Each NMR tube included an enclosed small tube containing a mixture of acetone-$d_6$/acetone-$h_6$ (9/1), which served as a reference for calibration. The NMR tubes were submerged in an ice bath (Figure S1, Supporting Information). Thermodynamically, THF-$d_8$ should form at 0 °C and 1 atm,[29,30] but we observed no clathrate formation in the NMR tubes even after 1 month, presumably due to the metastability of the solution. Hence, we added some tiny THF-$d_8$ crystals (formed by freezing the solution at −20 °C) to the THF-$d_8$ solution in the NMR tubes. With the seeds, THF-$d_8$ clathrate formed and grew slowly in each NMR tube. After 1 week, the samples were taken from the ice bath and stored at −20 °C in a freezer for 1 day before being used in NMR experiments. We found that THF-$d_8$ clathrate prepared via slow crystallization at 0 °C provided reproducible NMR responses. In contrast, fast crystallization of the solution at −20 °C resulted in THF-$d_8$ clathrate with less consistent NMR results, i.e., the amount of liquid-like water varied slightly. THF-$d_8$ clathrates reported in this work were prepared via slow crystallization at 0 °C unless otherwise stated.

$C_5D_{10}$ clathrate was also formed at 0 °C and 1 atm.[31−33] However, as cyclopentane is immiscible in water, only a micrometer-thick clathrate layer is formed at the phase boundary.[32,33] We overcame this mass transfer problem using a homogenizer (ALTRA-TURRAX) to mix a solution of $C_5D_{10}$ and water (volume ratio, 1:1) at a stirring speed of 15 000 rpm under 0 °C and 1 atm. The volume of $C_5D_{10}$ used was larger than the stoichiometric amount to avoid residual water, thereby avoiding the formation of ice in later stages. Solid clathrate was seen in the mixture after 5 min of mixing. The mixing process was continued for another 15 min. As a test, we also stirred pure water under the same conditions for 15 min and did not observe any solid in this case. The resulting clathrate was kept without stirring in the ice bath for 1 day before it was separated from residual liquid $C_5D_{10}$ and kept at −20 °C in a freezer. In the freezer, the $C_5D_{10}$ clathrate was manually ground into a powder and fed into NMR tubes together with an enclosed small tube of acetone-$d_6$/acetone-$h_6$ (mole ratio, 9:1) for referencing purposes. Samples of pristine ice were prepared and investigated for comparison.

*NMR Measurements.* All specimens were referenced and locked with an external capillary tube containing a mixture of acetone-$d_6$ and acetone-$h_6$ (mole ratio, 9:1), chemical shift $\delta(^1H)$ = 2.8 ppm due to dipolar deshielding by the surrounding water tube (Figure 1a). For $^1$H NMR measurements, a 5 mm TBI $^1$H/X probe equipped with a $z$-gradient on the 700 MHz Bruker AVANCE III system was used. Sixteen transients were acquired using a 9.1 $\mu$s long 90° pulse and 138 000 Hz (200 ppm) spectral width together with a recycling delay of 3 s. The broad sweep width has to be used due to the very broad water signal. The control of the temperature was realized by a BSVT (Bruker Smart Variable Temperature controller) with an accuracy of ±0.1 K. Experiments were performed through a stepwise increase of the temperature starting at 253 K. Our time-dependent measurements showed that the THF-$d_8$ clathrate reached an equilibrium state after annealing at a constant temperature for 20 min for the temperature range below 275 K. Hence, in temperature-dependent experiments, the sample was kept for 30 min at each temperature before the measurement started.

*Differential Scanning Calorimetry (DSC) Experiments.* DSC experiments were carried out on a DSC instrument (Mettler Toledo DSC 3+). In each experiment, 80 mg of a THF-$d_8$ solution of a desired concentration was fed into a sample container. The thermal profile of each experiment included four stages: (1) decreasing the temperature from 298 to 233 K at a rate of −10 K min$^{-1}$, (2) maintaining the temperature at 233 K for 2 h to guarantee the formation of the clathrate, (3) increasing the temperature from 233 to 261 K at a rate of 1.0 K/min, and (4) increasing the temperature from 261 to 298 K at a rate of 0.1 K min$^{-1}$. Stage (4) involved the dissociation of the clathrate and was of interest.

## 3. RESULTS AND DISCUSSION

**3.1. Two Types of Mobile Water in THF Clathrates.** $^1$H NMR spectra of THF-$d_8$ clathrate show two temperature-



https://doi.org/10.1021/acs.jpcc.1c05531
J. Phys. Chem. C 2021, 125, 15751−15757

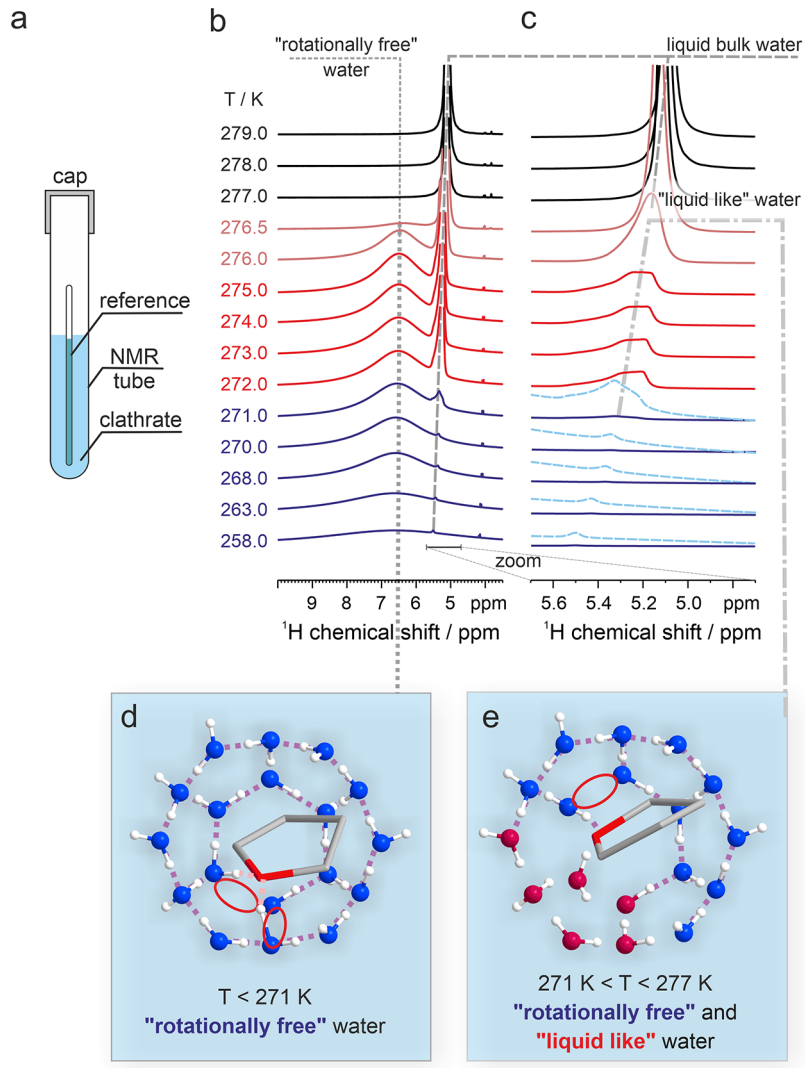


**Figure 1.** "Mobile" water molecules in THF-$d_8$ clathrate. (a) NMR tube containing the clathrate sample and an enclosed reference tube (acetone-$d_6$/acetone-$h_6$). (b) Temperature-dependent NMR spectra and (c) a detailed view of the chemical shift between 4.7 and 5.7 ppm. The spectral intensity is scaled with a factor 0.04 compared to (b) and only the spectra shown in dashed light blue lines are given on the same scale like (b) for comparison. (d) The peak at 6.5 ppm is attributed to reorienting H-bonded water molecules in the host structure induced by temporary host−guest H-bonding. The involved water molecules are partially uncoordinated with their neighbors and have a rotational freedom. The red ovals indicate the broken H-bonds between water molecules (L-type Bjerrum defects). Migration of Bjerrum defects in the cage makes all water molecules affected and become rotationally free in the time scale of milliseconds. Rotationally free water molecules are drawn in blue. (e) The peak at 5.2 ppm is ascribed to liquid-like water molecules that are extracted from the host matrix by the temporary host−guest H-bonds. The liquid-like water molecules are shown in red. Experiments were conducted through a stepwise increase of the temperature. The sample was kept at each temperature for 30 min before the measurement started. The referenced signal of acetone (2.8 ppm) is out of the plotting range.

dependent peaks: A broad peak at 6.5 ppm and a narrow one at around 5.2 ppm (Figure 1b,c). As only mobile water molecules can be observed in liquid-state $^1$H NMR spectra,[28] the occurrence of the two peaks provides direct signatures of mobile water molecules in the THF-$d_8$ clathrate. The peak at 6.5 ppm is pronounced in the region between 258 and 276.0 K, although it remains observable for temperatures down to 238 K. Thus, the mobile water molecules associated with this peak exist at temperatures far below the apparent equilibrium dissociation point (277 K) of the clathrate. This peak vanishes at temperatures from 277.0 K to higher. The narrow peak at 5.2 ppm starts occurring at 271.0 K and grows slightly until $T$ = 276.0 K, where it transforms into the signal of bulk liquid water (Figure 1c). In the following, we will explore the origin of these mobile water species.

We attribute the peak at 6.5 ppm to reorienting H-bonded water molecules in the host structure induced by the H-bonding defects originating from temporary host−guest H-bonding. The formation of water−THF H-bonding was predicted by molecular dynamics simulations.[19−22] Ethereal oxygen atom(s) on the polar guest molecules can form temporary H-bonds with water molecules in the host framework.[19−22] However, every water molecule is fully coordinated to their neighbors. The formation of temporary additional host−guest H-bonding therefore induces a local breakage of the intrinsic H-bonding between water molecules, which can be seen as L-type Bjerrum defects (red ovals in Figure 1d,e). Consequently, water molecules in the host framework of THF-$d_8$ clathrate are temporarily uncoordinated with at least one of their neighboring water molecules so that


https://doi.org/10.1021/acs.jpcc.1c05531
J. Phys. Chem. C 2021, 125, 15751−15757

the water molecules can reorient and coordinate with other neighbors. We note that these reorienting water molecules do not show translational motion, rather, they always stay H-bonded to the host lattice. However, if this tetrahedral reorientation of the water molecules is fast enough, then it averages out orientation-dependent, anisotropic NMR interactions and thus reduces the line broadening of the NMR signals. All of these dynamic processes are probed by $^1$H NMR on a millisecond time scale and are the origin of the peak at 6.5 ppm in Figure 1.

In other words, the signal at 6.5 ppm indicates water molecules that are incorporated and H-bonded to the host framework, but at the same time, they are already free to reorient in their tetrahedral environment. These mobile water molecules are, therefore, termed here as rotationally free water. To confirm this interpretation that the reorientation motion of water molecules in THF clathrates is initiated by fluctuating H-bonds to the polar site of the guest molecule, we compared liquid $^1$H NMR spectra of THF-$d_8$ clathrate, cyclopentane-$d_{10}$ clathrate, and pristine ice at 263 K (Figure 2). All spectra show

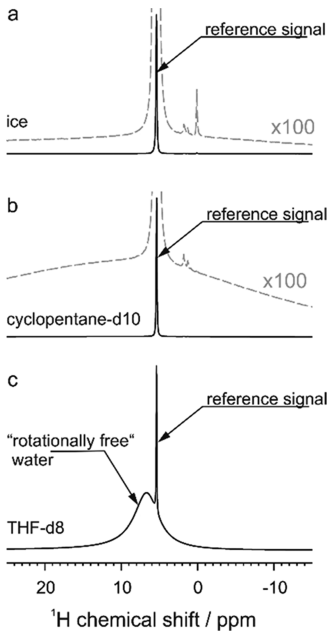


**Figure 2.** $^1$H NMR spectra recorded at 263 K for (a) pristine ice, (b) cyclopentane-$d_{10}$ clathrate, and (c) THF-$d_8$ clathrate plotted at the same scale (black solid lines). Magnified $^1$H NMR spectra are shown in dashed lines. Significant signature of rotationally free water is observed exclusively in THF-$d_8$ clathrate. Reference signal in this case was given by a mixture of $CD_2Cl_2$ and $CH_2Cl_2$ (mole ratio, 1:1).

a sharp peak at 5.4 ppm, originating from the referenced tube, in this case a mixture of $CD_2Cl_2/CH_2Cl_2$ (mole ratio 1/1). We used $CD_2Cl_2/CH_2Cl_2$ as a reference in early experiments before we realized that the $^1$H NMR signal of this reference (5.4 ppm) overlaps with the signals of THF-$d_8$ clathrate and creates difficulties for quantitative analysis. Therefore, we changed to the acetone reference in later experiments to avoid such overlapping. Nevertheless, the $CD_2Cl_2/CH_2Cl_2$ reference is sufficient for a qualitative discussion (Figure 2). The spectra of ice and $C_5D_{10}$ clathrate are very similar. Only at a 100-fold magnification, a broad signal of the $C_5D_{10}$ clathrate seems to be visible. It suggests a very low residual reorientation dynamics of water molecules in the cyclopentane clathrate originating from the additional host−guest interface of the clathrate in comparison to ice. Only the spectrum of THF-$d_8$ clathrate shows a clear signal at 6.5 ppm, demonstrating that only THF-$d_8$ clathrate has a significant amount of rotationally free water at 263.0 K.

At temperatures above 271.0 K, the interaction of the polar site of the THF-$d_8$ molecules with the host framework becomes strong enough to extract individual water molecules from the host framework (Figure 1e). The extracted water molecules are no longer H-bonded to the host structure but are translationally restricted to the cavity (red water molecules in Figure 1e). The formation of these water molecules starting at 271.0 K is observed in the $^1$H NMR spectra via the appearance of a second peak at 5.2 ppm. The fact that the position of this peak is close to the signal of bulk liquid water confirms the liquid-like feature of the extracted water molecules (Figure 1c). Thus, the peak at 5.2 ppm is assigned to liquid-like water molecules that are extracted from the host lattice by THF−water H-bonding.

**3.2. Fraction of Liquid-like Water and Two-Stage Dissociation Mechanism.** Both "rotationally free" water and liquid-like water exist in THF-$d_8$ clathrate in the temperature range of 271.0−277.0 K. We advance this finding by quantifying their fractions as a function of the temperature. Based on deconvolution of the NMR spectra, we determined the relative intensities of the signals of rotationally free water, liquid-like water, and the acetone reference. The referenced signal (acetone) stays constant throughout the whole range of investigated temperatures (Figure 3a). Interestingly, the total water signal, that is the sum of the intensities of the two water peaks, remains constant throughout the whole range of temperature (Figure 3a). We subtracted the referenced signal and calculated the normalized signal of rotationally free water and liquid-like water, i.e., the intensity of each water peak divided by the sum of the intensities of the two water peaks. This normalized intensity indicates the fraction of each type of water in the clathrate sample (Figure 3b). Evidently, liquid-like water molecules start occurring suddenly at around 271.0 K. One-third of total water molecules are converted into liquid-like at 271.0 K. The fraction then increases gradually to 45% at 276.0 K before rising vertically to 1.0 at 277.0 K

The present results reveal a two-stage dissociation of the THF-$d_8$ clathrate. The first stage occurs at 271.0 K and converts around 33% of total water molecules into a liquid-like state (Figure 1e). The second stage starts at 276.0 K and completes at 277.0 K, which converts the remaining clathrate structure into a liquid solution. It means that the THF-$d_8$ clathrate has a heterogeneous structure in the region between 271.0 and 277.0 K (Figure 1e). The temperature of the second stage (277.0 K) agrees well with the known apparent equilibrium dissociation point of THF clathrates.[34−36]

Our finding of the two-stage dissociation is complemented by differential scanning calorimetry (DSC) experiments. The DSC result shows two-phase transitions in the THF clathrate (Figure 3c). These DSC signals are well reproduced (Figure S2, Supporting Information). The DSC signal of transition I is symmetric and is fitted well by a Gaussian function (Figure 3c). Subtracting the signal of transition I from the DSC curve and then extrapolating the signal of transition II to lower temperatures indicate that both transitions have an identical onset temperature at around 271.0 K (Figure 3c). In the literature, transition I observed in the DSC curve was attributed to the melting of ice as a contaminant in THF


https://doi.org/10.1021/acs.jpcc.1c05531
J. Phys. Chem. C 2021, 125, 15751−15757

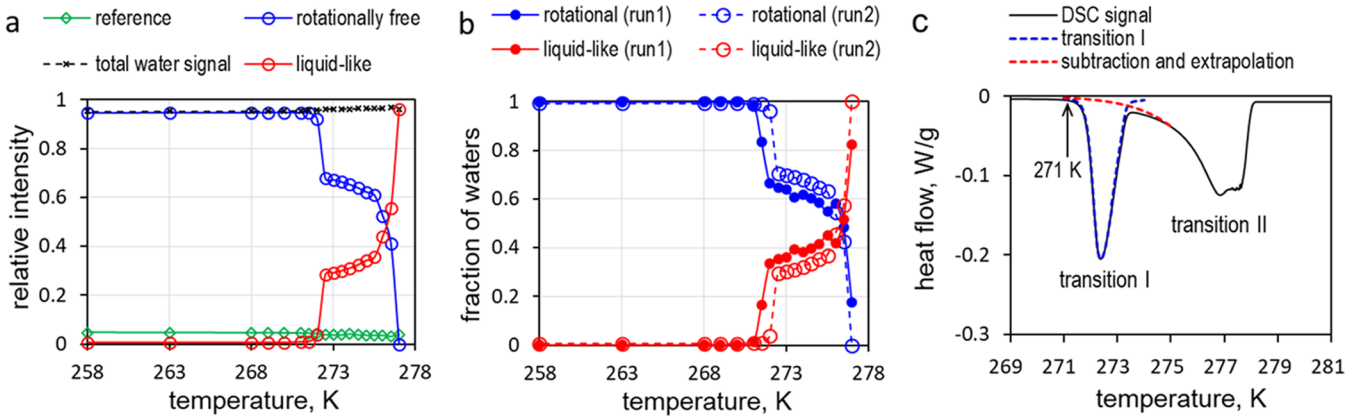


**Figure 3.** Two types of water in THF-$d_8$ clathrate. (a) Temperature-dependent signals of the referenced acetone, rotationally free water, and liquid-like water in THF-$d_8$ clathrate. The intensity of the referenced acetone signal stays constant for all temperatures. The sum of water signals also remains constant. (b) Normalized fraction of rotationally free water and liquid-like water in THF-$d_8$ clathrate by subtracting the referenced signal. Run1 and run2 indicate two examples of independent experiments. (c) Two-phase transitions observed in the DSC diagram show excellent agreement with the NMR results.

clathrate.[37,38] However, the onset temperature of transition I is typically below the melting point of pure ice. Some researchers, therefore, attributed this transition to the melting of a eutectic solid solution of THF and water.[36,39] Even so, the eutectic composition of THF−water solution is 10 wt % THF,[36] while our DSC experiments indicate that transition I can be measured up to a mixture containing 25 wt % THF-$d_8$ (Figure S3, Supporting Information). Thus, it is unclear how a eutectic composition of 10 wt % THF-$d_8$ could form in a solution of 25 wt % THF-$d_8$. More importantly, it is hard to differentiate the molecular structure of a eutectic THF−water solution from a THF clathrate.

The DSC result supports the two-stage dissociation mechanism of THF-$d_8$ clathrate observed in our NMR experiments. Both DSC and NMR data show an identical onset of transition I at 271.0 K (Figure 3). Moreover, the integrated areas of transition I and transition II in the DSC diagram reflect how much of the sample mass is dissociated in each transition. These areas are 0.19 W °C $g^{-1}$ and 0.27 W °C $g^{-1}$, respectively. Thus, 41% of the sample mass was dissociated in transition I and the rest was done in transition II. Meanwhile, the fraction of liquid-like water provides another measure of the dissociated portion of the clathrate in each transition. Figure 3b shows that between 33% (at 271.0 K) and 45% (up to 276.0 K) of the clathrate mass was dissociated in transition I. The exact value depends on the temperature at which transition I is considered complete. Hence, DSC and NMR results show a quantitative agreement and confirm the two-stage dissociation mechanism of THF-$d_8$ clathrate.

**3.3. Ruling Out the Presence of Ice in Stoichiometric THF Clathrates.** We have established a two-stage dissociation mechanism of THF-$d_8$ clathrate based on the two-phase transitions observed consistently in our NMR and DSC results. We further strengthen this interpretation by performing NMR experiments on a nonstoichiometric sample containing 2.3 wt % THF-$d_8$, i.e., much lower than the stoichiometric concentration of 20.7 wt %. This sample certainly contains ice due to the insufficient amount of THF-$d_8$. We calculated the sum of the signals of rotationally free water and liquid-like water relative to the referenced signal, similar to Figure 3a. The obtained results are compared to that of stoichiometric THF-$d_8$ clathrate (Figure 4).

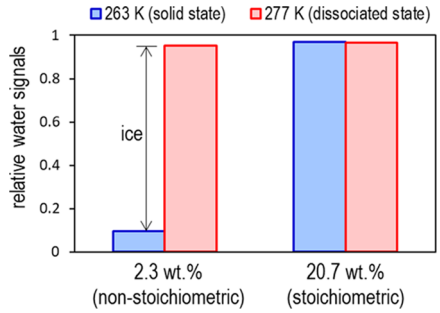


**Figure 4.** Total water signals relative to the reference signal recorded on a frozen mixture containing 2.3 wt % THF-$d_8$ and a stoichiometric THF-$d_8$ clathrate. The increase of total water signals upon dissociation in the first system proves the inclusion of ice in this mixture. The conservation of total water signals upon dissociation in the second system demonstrates no ice included in our THF-$d_8$ clathrate sample. The nonstoichiometric mixture was prepared via freezing a corresponding solution at −20 °C.

As shown in Figure 3a for a stoichiometric THF-$d_8$ clathrate, the sum of water signals remains constant upon dissociation. For example, the sum of water signals at any temperature prior to dissociation (e.g., at 263 K) is equal to that at any temperature after dissociation (e.g., at 277 K) for a stoichiometric THF-$d_8$ clathrate (Figure 4). The fact that the sum of water signals remains constant upon dissociation of a stoichiometric THF-$d_8$ clathrate indicates that all water molecules in the clathrate sample are "visible" in the $^1$H NMR spectra at all temperatures investigated. There are no NMR-inactive water molecules in the THF-$d_8$ clathrate. Physically, it means that all water molecules in the clathrate lattice undergo reorientation motion on the millisecond time scale and contribute to the NMR signals. This finding is consistent in part with previous claims based on solid-state experiments that the structure of THF clathrate associates with a lower activation barrier for the reorientation of water molecules and a more labile water framework in comparison to ice.[25,26] Even though the new physical insight of our finding is


https://doi.org/10.1021/acs.jpcc.1c05531
J. Phys. Chem. C 2021, 125, 15751−15757

that all water molecules in THF-$d_8$ clathrate are rotationally free in the time scale of milliseconds.

Unlike the stoichiometric THF-$d_8$ clathrate, the non-stoichiometric sample shows a substantial increase of water signals upon dissociation. It indicates that this sample contains a large amount of ice. The "invisibility" of ice in the $^1$H NMR spectra (Figure 2) is the reason of the reduced water signals at 263 K (Figure 4). The melting of ice produces liquid water that adds up signals to the total water signals. Therefore, the inclusion of ice in the sample leads to an increase of total water signals upon dissociation of the sample (Figure 4). In contrast, the conversion of total water signals upon the dissociation of the stoichiometric THF-$d_8$ clathrate confirms no ice included in our clathrate samples. Hence, the transition I in the DSC diagram is not given by the melting of ice, which is in contrast to the common consensus. Instead, the two transitions observed in the DSC diagram support the two-stage dissociation mechanism of the THF-$d_8$ clathrate we established based on our NMR results. Finally, we note that clathrates of nondeuterated THF ($C_4H_8O$) and cyclopentane ($C_5H_{10}$) exhibit similar NMR behaviors to their deuterated versions except that additional signals of $^1$H protons in nondeuterated guest molecules complicate the spectra (Figure S4, Supporting Information) and minor shifts in the transition temperatures.

**3.4. Significance of the Present Findings.** Our findings help us to elucidate the stability of clathrates. For example, cyclopentane, THF, and 1,3-dioxolane have similar molecular sizes, shapes, and molecular weights. However, cyclopentane has no ethereal oxygen atom while THF has one oxygen atom and 1,3-dioxolane has two. The ethereal oxygen atom(s) destabilizes the clathrate structures via temporary host−guest H-bonding. We, therefore, expect the thermodynamic stability of these clathrates to follow the order: cyclopentane clathrate > THF clathrate > 1,3-dioxolane clathrate. This prediction is confirmed by the decrease of the equilibrium melting temperature ($T_e$) in a similar sequence: cyclopentane clathrate ($T_e$ = 280.8 K), THF clathrate (277.0 K), and 1,3-dioxolane clathrate (270.1 K).[34,35,40−42]

In addition, the present findings might be useful for developing capable methods for recovering methane from natural clathrates. Extracting methane from natural clathrates requires appropriate measures to destabilize the clathrate structure so that it dissociates and liberates methane.[9] Two potential ways to destabilize the clathrate deposits have been proposed in the literature based on the depressurization and thermal stimulation (heating) processes.[9] In the light of present results, the injection of appropriate structural disruptors (polar chemicals) into clathrate deposits may induce synergistic effects on depressurization or thermal stimulation processes. The injected chemicals weaken the clathrate structures and make the depressurization or thermal stimulation processes more energy-efficient. However, additional harmful side effects on the nature due to the injection of chemicals have to be considered.

## 4. CONCLUSIONS

Appropriately designed liquid-state $^1$H NMR experiments with an external reference enabled us to directly observe and quantify the formation of liquid-like water molecules in clathrates containing polar guest molecules. We demonstrated that all water molecules in THF clathrates are rotationally free on the time scales between microseconds and milliseconds in our NMR experiments. The structure of THF clathrates is heterogeneous in the temperature region between 271.0 and 277.0 K as featured by the concurrent presence of rotationally free water and liquid-like water. We revealed a two-stage dissociation of THF clathrate and proposed a temperature-dependent molecular structure of this clathrate. This work indicated that liquid-state NMR is a powerful technique for studying the structure and dynamics of clathrates. The present findings provide a breakthrough in clathrate science and the allied fields such as physiochemical and biological processes where host−guest interaction plays a role.

## ■ ASSOCIATED CONTENT

### Supporting Information

The Supporting Information is available free of charge at https://pubs.acs.org/doi/10.1021/acs.jpcc.1c05531.

Preparation of THF-$d_8$ clathrates in an ice bath; DSC curves for different THF-$d_8$ concentrations; and $^1$H NMR spectra for nondeuterated guest molecules (PDF)

## ■ AUTHOR INFORMATION


### Corresponding Authors

**Ngoc N. Nguyen** − *Max Planck Institute for Polymer Research, 55128 Mainz, Germany; Hanoi University of Science and Technology, Hanoi 100000, Vietnam;* orcid.org/0000-0002-0999-1176; Email: nguyenn@mpip-mainz.mpg.de

**Rüdiger Berger** − *Max Planck Institute for Polymer Research, 55128 Mainz, Germany;* orcid.org/0000-0002-4084-0675; Email: berger@mpip-mainz.mpg.de

**Robert Graf** − *Max Planck Institute for Polymer Research, 55128 Mainz, Germany;* orcid.org/0000-0003-2302-0760; Email: graf@mpip-mainz.mpg.de

### Authors

**Manfred Wagner** − *Max Planck Institute for Polymer Research, 55128 Mainz, Germany*

**Jürgen Thiel** − *Max Planck Institute for Polymer Research, 55128 Mainz, Germany*

**Hans-Jürgen Butt** − *Max Planck Institute for Polymer Research, 55128 Mainz, Germany;* orcid.org/0000-0001-5391-2618

Complete contact information is available at: https://pubs.acs.org/10.1021/acs.jpcc.1c05531


### Notes

The authors declare no competing financial interest.

## ■ ACKNOWLEDGMENTS

N.N.N. gratefully acknowledges the Alexander von Humboldt (AvH) Foundation for the AvH Fellowship for Postdoctoral Researchers (Fellowship Number: VNM 1200537 HFST-P). The authors thank Uwe Rietzler, Stefan Spang, Marc-Jan van Zadel, and Helma Burg for their technical assistance.

## ■ REFERENCES

(1) Gupta, A.; Baron, G. V.; Perreault, P.; Lenaerts, S.; Ciocarlan, R.-G.; Cool, P.; Mileo, P. G. M.; Rogge, S.; Van Speybroeck, V.; Watson, G.; et al. M. Hydrogen Clathrates: Next Generation Hydrogen Storage Materials. *Energy Storage Mater.* **2021**, *41*, 69−107.

(2) Both, A. K.; Gao, Y.; Zeng, X. C.; Cheung, C. L. Gas Hydrates in Confined Space of Nanoporous Materials: New Frontier in Gas Storage Technology. *Nanoscale* **2021**, *13*, 7447−7470.

(3) Wang, W. X.; Bray, C. L.; Adams, D. J.; Cooper, A. I. Methane Storage in Dry Water Gas Hydrates. *J. Am. Chem. Soc.* **2008**, *130*, 11608−11609.
(4) Cuadrado-Collados, C.; Mouchaham, G.; Daemen, L.; Cheng, Y.; Ramirez-Cuesta, A.; Aggarwal, H.; Missyul, A.; Eddaoudi, M.; Belmabkhout, Y.; Silvestre-Albero, J. Quest for an Optimal Methane Hydrate Formation in the Pores of Hydrolytically Stable Metal−Organic Frameworks. *J. Am. Chem. Soc.* **2020**, *142*, 13391−13397.
(5) Sloan, E. D. Fundamental Principles and Applications of Natural Gas Hydrates. *Nature* **2003**, *426*, 353−359.
(6) Nguyen, N. N.; Galib, M.; Nguyen, A. V. Critical Review on Gas Hydrate Formation at Solid Surfaces and in Confined Spaces—Why and How Does Interfacial Regime Matter? *Energy Fuels* **2020**, *34*, 6751−6760.
(7) Klauda, J. B.; Sandler, S. I. Global Distribution of Methane Hydrate in Ocean Sediment. *Energy Fuels* **2005**, *19*, 459−470.
(8) Giavarini, C.; Hester, K. *Gas Hydrates: Immense Energy Potential and Environmental Challenges*; Springer London: London, 2011; pp 1−175.
(9) Hassanpouryouzband, A.; Joonaki, E.; Vasheghani Farahani, M.; Takeya, S.; Ruppel, C.; Yang, J.; English, N. J.; Schicks, J. M.; Edlmann, K.; Mehrabian, H.; et al. Gas Hydrates in Sustainable Chemistry. *Chem. Soc. Rev.* **2020**, *49*, 5225−5309.
(10) Brewer, P. G. Gas Hydrates and Global Climate change. *Ann. N. Y. Acad. Sci.* **2000**, *912*, 195−199.
(11) Ruppel, C. D.; Kessler, J. D. The Interaction of Climate Change and Methane Hydrates. *Rev. Geophys.* **2017**, *55*, 126−168.
(12) Englezos, P. Clathrate Hydrates. *Ind. Eng. Chem. Res.* **1993**, *32*, 1251−1274.
(13) Nguyen, N. N.; Berger, R.; Butt, H.-J. Premelting-Induced Agglomeration of Hydrates: Theoretical Analysis and Modeling. *ACS Appl. Mater. Interfaces* **2020**, *12*, 14599−14606.
(14) Bhattacharjee, G.; Goh, M. N.; Arumuganainar, S. E. K.; Zhang, Y.; Linga, P. Ultra-rapid Uptake and the Highly Stable Storage of Methane as Combustible Ice. *Energy Environ. Sci.* **2020**, *13*, 4946−4961.
(15) Koh, C. A.; Sloan, E. D.; Sum, A. K.; Wu, D. T. Fundamentals and Applications of Gas Hydrates. *Annu. Rev. Chem. Biomol. Eng.* **2011**, *2*, 237−257.
(16) Lee, H.; Lee, J. W.; Kim, D. Y.; Park, J.; Seo, Y. T.; Zeng, H.; Moudrakovski, I. L.; Ratcliffe, C. I.; Ripmeester, J. A. Tuning Clathrate Hydrates for Hydrogen Storage. *Nature* **2005**, *434*, 743−746.
(17) Nguyen, N. N.; Berger, R.; Butt, H.-J. Surface Premelting and Interfacial Interactions of Semi-Clathrate Hydrate. *J Phys. Chem. C* **2019**, *123*, 24080−24086.
(18) Nguyen, T. T.; Pétuya, C.; Talaga, D.; Desmedt, A. Promoting the Insertion of Molecular Hydrogen in Tetrahydrofuran Hydrate With the Help of Acidic Additives. *Front. Chem.* **2020**, *8*, No. 920.
(19) Mohammadi-Manesh, H.; Ghafari, H.; Alavi, S. Molecular Dynamics Study of Guest−Host Hydrogen Bonding in Ethylene Oxide, Trimethylene Oxide, and Formaldehyde Structure I Clathrate Hydrates. *J. Phys. Chem. C* **2017**, *121*, 8832−8840.
(20) Kulig, W.; Kubisiak, P.; Cwiklik, L. Steric and Electronic Effects in the Host−Guest Hydrogen Bonding in Clathrate Hydrates. *J. Phys. Chem. A* **2011**, *115*, 6149−6154.
(21) Alavi, S.; Susilo, R.; Ripmeester, J. A. Linking Microscopic Guest Properties to Macroscopic Observables in Clathrate Hydrates: Guest-Host hydrogen Bonding. *J. Chem. Phys.* **2009**, *130*, No. 174501.
(22) Alavi, S.; Udachin, K.; Ripmeester, J. A. Effect of Guest−Host Hydrogen Bonding on the Structures and Properties of Clathrate Hydrates. *Chem. - Eur. J.* **2010**, *16*, 1017−1025.
(23) Kirschgen, T. M.; Zeidler, M. D.; Geil, B.; Fujara, F. A Deuteron NMR Study of the Tetrahydrofuran Clathrate Hydrate Part II: Coupling of Rotational and Translational Dynamics of Water. *Phys. Chem. Chem. Phys.* **2003**, *5*, 5247−5252.
(24) Bach-Vergés, M.; Kitchin, S. J.; Harris, K. D. M.; Zugic, M.; Koh, C. A. Dynamic Properties of the Tetrahydrofuran Clathrate Hydrate, Investigated by Solid State 2H NMR Spectroscopy. *J. Phys. Chem. B* **2001**, *105*, 2699−2706.
(25) Gough, S. R.; Hawkins, R. E.; Morris, B.; Davidson, D. W. Dielectric Properties of Some Clathrate Hydrates of Structure II. *J. Phys. Chem. A* **1973**, *77*, 2969−2976.
(26) Ba, Y.; Ripmeester, J. A.; Ratcliffe, C. I. Water Molecular Reorientation in Ice and Tetrahydrofuran Clathrate Hydrate from Lineshape Analysis of $^{17}O$ Spin-echo NMR Spectra. *Can. J. Chem.* **2011**, *89*, 1055−1064.
(27) Sengupta, S.; Guo, J.; Janda, K. C.; Martin, R. W. Exploring Dynamics and Cage−Guest Interactions in Clathrate Hydrates Using Solid-State NMR. *J. Phys. Chem. B* **2015**, *119*, 15485−15492.
(28) Gun'ko, V. M.; Turov, V. V.; Bogatyrev, V. M.; Zarko, V. I.; Leboda, R.; Goncharuk, E. V.; Novza, A. A.; Turov, A. V.; Chuiko, A. A. Unusual Properties of Water at Hydrophilic/Hydrophobic Interfaces. *Adv. Colloid Interface Sci.* **2005**, *118*, 125−172.
(29) Seo, Y.-T.; Lee, H.; Moudrakovski, I.; Ripmeester, J. A. Phase Behavior and Structural Characterization of Coexisting Pure and Mixed Clathrate Hydrates. *ChemPhysChem* **2003**, *4*, 379−382.
(30) Strauch, B.; Schicks, J. M.; Luzi-Helbing, M.; Naumann, R.; Herbst, M. The Difference between Aspired and Acquired Hydrate Volumes − A Laboratory Study of THF Hydrate Formation in Dependence on Initial THF:$H_2O$ Ratios. *J. Chem. Thermodyn.* **2018**, *117*, 193−204.
(31) Nakajima, M.; Ohmura, R.; Mori, Y. H. Clathrate Hydrate Formation from Cyclopentane-in-Water Emulsions. *Ind. Eng. Chem. Res.* **2008**, *47*, 8933−8939.
(32) Dann, K.; Rosenfeld, L. Surfactant Effect on Hydrate Crystallization at the Oil−Water Interface. *Langmuir* **2018**, *34*, 6085−6094.
(33) Sakemoto, R.; Sakamoto, H.; Shiraiwa, K.; Ohmura, R.; Uchida, T. Clathrate Hydrate Crystal Growth at the Seawater/Hydrophobic−Guest−Liquid Interface. *Cryst. Growth Des.* **2010**, *10*, 1296−1300.
(34) Bollavaram, P.; Devarakonda, S.; Selim, M. S.; Sloan, E. D. Growth Kinetics of Single Crystal sII Hydrates: Elimination of Mass and Heat Transfer Effects. *Ann. N. Y. Acad. Sci.* **2000**, *912*, 533−543.
(35) Makino, T.; Sugahara, T.; Ohgaki, K. Stability Boundaries of Tetrahydrofuran + Water System. *J. Chem. Eng. Data* **2005**, *50*, 2058−2060.
(36) Jones, C. Y.; Zhang, J.; Lee, J. W. Isotope Effect on Eutectic and Hydrate Melting Temperatures in the Water-THF System. *J. Thermodyn.* **2010**, *2010*, 1−6.
(37) Zhang, Y.; Debenedetti, P. G.; Prud'homm, R. K.; Pethica, B. A. Differential Scanning Calorimetry Studies of Clathrate Hydrate Formation. *J. Phys. Chem. B* **2004**, *108*, 16717−16722.
(38) Kumar, A.; Kumar, R.; Linga, P. Sodium Dodecyl Sulfate Preferentially Promotes Enclathration of Methane in Mixed Methane-Tetrahydrofuran Hydrates. *iScience* **2019**, *14*, 136−146.
(39) Delahaye, A.; Fournaison, L.; Marinhas, S.; Chatti, I.; Petitet, J.-P.; Dalmazzone, D.; Fürst, W. Effect of THF on Equilibrium Pressure and Dissociation Enthalpy of $CO_2$ Hydrates Applied to Secondary Refrigeration. *Ind. Eng. Chem. Res.* **2006**, *45*, 391−397.
(40) Aspenes, G.; Dieker, L. E.; Aman, Z. M.; Høiland, S.; Sum, A. K.; Koh, C. A.; Sloan, E. D. Adhesion Force between Cyclopentane Hydrates and Solid Surface Materials. *J. Colloid Interface Sci.* **2010**, *343*, 529−536.
(41) Dyadin, Y. A.; Zhurko, F. V.; Bondaryuk, I. V.; Zhurko, G. O. Clathrate Formation in Water-Cyclic Ether Systems at High Pressures. *J. Inclusion Phenom. Mol. Recognit. Chem.* **1991**, *10*, 39−56.
(42) Venkateswaran, A.; Easterfield, J. R.; Davidson, D. W. A Clathrate Hydrate of 1,3-Dioxolane. *Can. J. Chem.* **1967**, *45*, 884−886.


https://doi.org/10.1021/acs.jpcc.1c05531
J. Phys. Chem. C 2021, 125, 15751−15757